Sensitivity of engineering demand parameters as a function of structural typology and assessment method

A. Stocchi, B. Richard

▶ **To cite this version:**

A. Stocchi, B. Richard. Sensitivity of engineering demand parameters as a function of structural typology and assessment method. Nuclear Engineering and Design, 2019, 343, pp.151-165. 10.1016/j.nucengdes.2019.01.006 . hal-02521637

HAL Id: hal-02521637
https://hal.science/hal-02521637

Submitted on 21 Oct 2021

HAL is a multi-disciplinary open access archive for the deposit and dissemination of scientific research documents, whether they are published or not. The documents may come from teaching and research institutions in France or abroad, or from public or private research centers.

L'archive ouverte pluridisciplinaire **HAL**, est destinée au dépôt et à la diffusion de documents scientifiques de niveau recherche, publiés ou non, émanant des établissements d'enseignement et de recherche français ou étrangers, des laboratoires publics ou privés.

Distributed under a Creative Commons Attribution - NonCommercial 4.0 International License

Version of Record: https://www.sciencedirect.com/science/article/pii/S0029549318309750
Manuscript_2cde3cd39da781e1ab06a600943285fc

Sensitivity of engineering demand parameters as a function of structural typology and assessment method

Alessandro Stocchi[a], Benjamin Richard[b,*]

[a]*DEN - Service d'Études Mécaniques et Thermiques (SEMT), CEA, Université Paris-Saclay, F-91191 Gif sur Yvette, France.*
[b]*IRSN, 31 avenue du Général Leclerc, F-92269 Fontenay-aux-Roses, France.*

Abstract

Fragility curves express the failure probability of a structure, or a critical component, as a function of a seismic intensity measure, for a given failure criterion. The failure criterion is often built as the difference between a structural response and a threshold, which can be either deterministic or probabilistic. Within a probabilistic context, the structural response is a random variable and therefore, it will be subjected to a certain variability mostly depending on the structural typology and the assessment method. When engineers have to make a decision to choose the appropriate engineering demand parameter to consider, they need to know how much sensitive it will be. The study reported in this paper attempts to bring answers to this question. More precisely, the sensitivity of some engineering demand parameters is quantified and discussed as a function of the structural typology (beam-column or wall-based structures) and of the considered assessment method. The final output is a correlation matrix linking (i) the coefficient of variation of specific engineering demand parameters, (ii) the structural typology and (iii) the type of assessment method.

Keywords: Time history analysis, probabilistic, non linear analysis, seismic assessment, engineering demand parameters

1. Introduction

The seismic Probabilistic Risk Assessment (PRA) methodology has become highly used in the nuclear industry for the estimation of the seismic risk of Nuclear Power Plants (NPPs) [1]. In the PRA approach, fragility curves are computed as conditional probabilities of failure of structures, or critical components, for given values of a seismic Intensity Measure (IM) [2]. More precisely, the fragility is defined as follows:

$$P_f(\alpha) = P(y - y_0 > 0 \mid \alpha) \tag{1}$$

where P_f is the probability of failure, α stands of the IM characterizing the seismic loading, y describes the structural response, translated into the Engineering Demand Parameter (EDP) and y_0 is a given threshold which is used to define the concept of failure. From this definition, it is clear that the nature of the IM, the type (force, displacement, etc.) of quantity y and the value of y_0 are chosen by the user. Hence, the fragility curve estimation requires (i) a probabilistic model which consists in choosing a set of random variables with associated Probability Density Functions (PDF), (ii) an uncertainty propagation method and (iii) a mechanical model to describe the structural outputs [3]. How to choose the random model and which uncertainty propagation technique to consider are crucial questions which have been addressed for the past decades by the scientific community. For instance, several interesting works have been proposed to improve the efficiency of the propagation methods in order to decrease its computational demand when evaluating the

*Corresponding author
Email addresses: Alessandro.Stocchi@cea.fr (Alessandro Stocchi), Benjamin.Richard@irsn.fr (Benjamin Richard)

© 2019 published by Elsevier. This manuscript is made available under the CC BY NC user license
https://creativecommons.org/licenses/by-nc/4.0/

mechanical model. Dedicated approach mostly based on log-normal assumptions of the fragility curves [4, 5] or on the construction of solver surrogates [6, 7] have been developed and successfully applied on complex structural case studies [5, 8, 9]. The last feature required when dealing with fragility curves computation is a mechanical model. Making assumptions is necessary when developing such a structural model. Sometimes, the geometry is simplified or the values of some unknown material parameters are assumed [10, 11]. This study aims to assess the influence of the assumptions made on the structural model on the variability of selected EDPs. In such a way, engineers in charge of developing structural models will be able to take benefits from the expected variability of the output quantities to select the appropriate EDP.

In the context of fragility curve estimation, the uncertainties are usually sorted in two categories. The first one gathers the aleatory uncertainties which attempts to describe the intrinsic random nature of the variables or processes involved in the analysis. The second one includes the epistemic uncertainties which represent the lack of knowledge about the used modelling technique [8]. Both types should be taken into account when evaluating a fragility curve, especially when confidence intervals are required. In practice, we can distinguish on one hand the seismic loading, which contributes in the aleatory part of uncertainties and, on the other hand, the so-called material or model parameters (material strengths, damping ratios, etc.), which contribute in the epistemic uncertainties. When a full probabilistic analysis is carried out, uncertainties associated with the seismic loading are naturally taken into account [12]. In this case, these uncertainties are often preponderant compared with the ones associated with the material parameters, as reported [13]. In addition, it is also reported that uncertainties related to the material parameters may have a strong influence, depending on the structural typology considered (masonry walls, RC beam-column structures, etc.). Several methodologies which aim at reducing the scatter in fragility curves computations by appropriate manipulations of input signals parameters were also developed in the last decade [14, 15]. These manipulations can be made dependent on the damage state of the considered structure. That is why the common engineering practice lies in setting up to zero the uncertainties related to the material parameters. The work carried out by [16] studied the weight of uncertainties related to the ground motion and to the material parameters. The authors concluded on the importance of the uncertainties related to the ground motion but did not consider the influence of the structural typology or of the assessment method. The work presented in this paper is in a similar line to the one performed by [16, 17]. Considering the ground motion as deterministic, the uncertainties related to the model parameters can be propagated and their resulting influence on the EDPs can be quantified, as a function of the structural typology and the modelling technique.

This paper is organized as follows. In section 2, the overall flowchart of the used analysis method is described. The probabilistic model is presented. The EDPs studied in the paper are also precised. Due to the wide range of possible EDPs to describe neither structural response nor an exhaustive study was possible. That is why the most used EDPs are considered. In section 3, the structural case-studies are presented. For the sake of completeness, a beam-columns and a shear-wall-based structure were considered. In such a way, the type of structural typology can be considered as a parameter [18] to study the sensitivity of the EDPs. For each type of structure, the corresponding mechanical models are described. The difference between each model is mainly related to the type of the mesh used, which corresponds to the engineering modelling practice and on the available time to spend on developing the model. The statistical convergence of the probabilistic study is also investigated. In section 4, the results are presented. Especially, the coefficients of variation of the EDPs are studies in conjunction with the structural typology and with the used type of modelling technique.

2. Flowchart of the analysis process

In this section, the probabilistic analysis conducted to study the sensitivity of the selected EDPs is described. It is composed of three steps. The first one consists in defining the random model. The variables to be considered as random are selected and the associated PDFs are chosen. The second step lies in making propagate the uncertainties through the deterministic mechanical model, which is assumed to be consistent

(at least in mean) with the physics involved in the problem. Based on the results of the second step, the last step consists in computing the selected EDPs.

2.1. The random model

Let us consider the following random variables $(X_1, \cdots, X_d)$, $d \in \mathbb{N}^\star$. We assume these variables are gathered in a random vector $\mathbf{X}$. They are defined by a multivariate probability density function $p_{\mathbf{X}}(\mathbf{x})$, with $\mathbf{x} = (x_1, \cdots, x_d)$ the corresponding realizations. For all mechanical models used in this study, we choose $d = 5$. In other words, five random variables are selected. Their physical meaning is and the associated PDFs are described in table 1. We can notice that log-normal PDFs were chosen, which is quite common when the support of the random variables must stay positive due to physical considerations. The mean values are not precised in table 1 since they depend on the structural case-study. That is why they are clarified in section 3. However, the statistical parameters (mean and coefficient of variation) have been identified from mechanical tests carried out on several small-scale samples. In addition, the fracture energy has also been considered to be a random variable even though is has not been measured by mechanical tests. This parameter has been estimated by analytic relationships available in [19]. As far as the generation of

Variable	Meaning	Distribution	Unit	Mean	COV (%)
E	Young's modulus	Log-normal	Pa	CD	15
G_f	Fracture energy	Log-normal	$J.m^{-3}$	CD	30
f_t	Tensile strength	Log-normal	Pa	CD	30
σ_e	Yield stress	Log-normal	Pa	CD	5
ξ	Damping ratio	Log-normal	$-$	CD	20

Table 1: Statistical parameters and PDFs of the random variables. CD = case-dependent, COV = coefficient of variation.

the realization of the random variables is concerned, the joint PDF is not used. Indeed, realizations of the random vector are generated in the normalized standard space, in which all the random variables are uncorrelated and follow the standard Gaussian probabilistic law. Then, the Rosenblatt's transform [20] is used to affect them a log-normal PDF. If correlation between random variables had been considered, the Nataf's [21] could have been used to take it into account. In the present study, no correlation is assumed. The histograms of the realizations of the input material parameters are presented in appendices A and B, depending on the case study. In accordance with the objectives of the present study, the ground motion is assumed to be deterministic.That is to say a unique set of accelerograms has been considered for each case-study (BANDIT and SMART 2013) to describe the seismic loading.

2.2. Mechanical model and uncertainty propagation technique

A mechanical model can be described according to equation 2:

$$\mathbf{y} = f(\mathbf{x}, a(t)) \tag{2}$$

where $\mathbf{y}$ stands for the vector of EDPs, a for the ground motion and t for the time. f is an algebraic operator that represents the used modelling approach, which is often derived from the Finite Element Method (FEM). With the aim to study the effects of both the structural typology, and the modelling technique, five different mechanical models have been defined. More in details, two structural typologies were selected: a Reinforced Concrete (RC) beam-column structure and a RC shear-wall-based structure. In case of the beam-column structure, three modelling strategies were considered. The main difference between them is the type of Finite Element (FE) used: Timoshenko's multifiber beam elements [22], mutilayer shell elements [23] and solid elements [24]. In case of the RC shear-wall-based structure, only two modelling strategies were considered. The reason for this choice is that modelling approaches based upon beam elements is not common in the engineering practice. The difference between the modelling strategies are the same as the ones mentioned

in case of the beam-column structure. Regarding the uncertainties propagation technique, the the well-known Monte Carlo Simulation Method (MCSM) has been used [25]. Despite the fact that it leads to a high computational demand, it has been used mainly because it allows an online control of the variance associated with the results. The statistical convergence can easily checked.

2.3. Engineering demand parameters

Six EDPs were selected. The selection criterion was based on the fact that they are commonly used in the engineering practice [26, 27, 10]. They are described in table 2. The Maximum Interstorey Drift Ratio

EDP acronym	Unit	Definition/physical meaning
MIDR	%	Maximum interstorey drift ratio
EFDO	%	Eigenfrequency drop off
DUCT	$(-)$	Ductility
DER	$(-)$	Hysteretic energy over total input energy
ZPA	$\mathrm{m.s}^{-2}$	Zero period acceleration
AMPR	$(-)$	Amplification ratio

Table 2: Definition of the selected EDPs.

(MIDR) is defined as the ratio between the in-plane displacements at two consecutive storeys over the height of the storey. This quantity is used to estimate the shear distribution in a given storey. In addition, many performance criteria are expressed by means of the index. The EigenFrequency Drop Off (EFDO) is less used than the MIDR. However, because eigenfrequencies are linked with the stiffness of a structure, the drop off can be interpreted as a structural damage index. Safety margin estimation and damage thresholds based upon the use of this index have been recently proposed [28, 29]. More precisely, the EFDO is computed in a very pragmatic way by means of a windowing technique. The damaged frequency corresponds to the local maximum of the acceleration spectrum on the lower frequencies domain with respect to the undamaged frequency. This was the only way to detect a damage frequency with sufficient accuracy on a large pool of spectra. The DUCTility (DUCT) index is defined as the ratio between the maximum displacement over the last value of the displacement for which the structure remains elastic. This quantity is often used in the context of structural assessment to verify that the structure is able to withstand to a given action (classically not taken in to account in the design stage), even if the index denominator is difficult to measure experimentally. Less classical than the other indices, the Hysteretic EneRgy over total input energy (DER) is useful to estimate the ratio of the energy which is dissipated by the constitutive materials themselves. It is defined as the ratio between the hysteretic energy over the total input energy. The hysteretic energy can be estimated from the internal variables of constitutive laws. The Zero Period Acceleration (ZPA) is defined as the pseudo-acceleration estimated either when the period is null or when the frequency tends to infinity. For some methodologies mainly devoted to equipment assessment, the ZPA allows for the load determination. The last selected EDP is the AMPlification Ratio (AMPR). It is defined as the ratio between the maximum pseudo-acceleration over the ZPA. The AMPR is introduced in some standards [30] to define the design spectrum.

3. Structural case-studies: experimental setup and modelling strategies

This section is devoted to the presentation of the two structures which are studied in this work. The structures have been chosen according three criteria: (i) the availability of experimental data, (ii) the accessibility of the test report and (iii) the fact they are representative of beam-column and shear-wall-based structures. Despite the fact that other structures could have been selected, the BANDIT [31, 32] and SMART 2013 [29, 33] RC structures were chosen because they respect the aforementioned criteria. In addition, both case-studies have been experimentally tested in order to improve knowledge of RC structures behavior encountered in civil engineering for nuclear applications.

Level number	Young modulus (MPa)	Poisson ratio (-)	Compressive strength (MPa)	Tensile strenght (MPa)	Density ($kg.m^{-3}$)
# 1	25200	0.19	30.5	2.3	2300
# 2	20400	0.19	23.0	2.3	2300

Table 3: Results from the mechanical test to characterize concrete - BANDIT.

3.1. BANDIT experiment as a beam-column structure

3.1.1. Experimental setup

The tested structure was a one-bay two-story frame building regular in plan and elevation, similar to a building tested as part of the Ecoleader research project [34, 35] and built according to substandard construction practices applicable in European countries. The design spectrum has been defined in accordance with Eurocode 8 [36]. It corresponds to 5% damping, a C-type soil, a type-II reference spectrum and a reference acceleration of 0.1 g. The category of importance has been set up to II. The resulting design spectrum is shown in figure 1a. The accelerogram considered for the seismic loading is shown in appendix C. The picture of the BANDIT structure is shown in figure 1b. Figure 2 shows details of the general

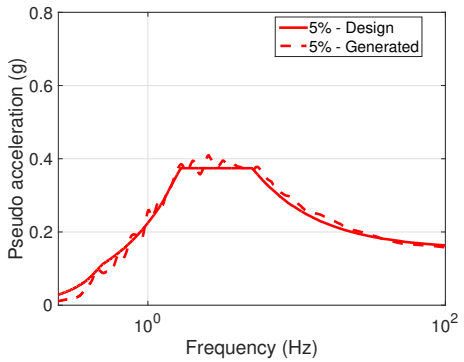

(a) Design spectrum.

(b) Picture of the BANDIT specimen.

Figure 1: Design spectrum and picture of the BANDIT specimen.

geometry of the BANDIT specimen. The building was 4.26×4.26 m^2 in plan and had a constant floor height of 3.30 m. The cross section of the columns was 260×260 mm^2. The first floor columns were reinforced with eight 14 mm deformed bars, whilst the second-floor columns had four 14 mm deformed bars. This resulted in longitudinal reinforcement ratios of 1.82% and 0.91% for the first-and second-floor columns, respectively. These relatively low ratios are typical of substandard columns of existing buildings. The reduction of longitudinal column reinforcement between floors was, and in some countries still is, a typical construction practice adopted to save material costs. The columns had transverse reinforcement consisting of 6 mm stirrups at 200 mm spacing. The stirrups were closed with 90 ° bends instead of 135 ° hooks required by current seismic codes. Concrete and steel reinforcing bars used to build the BANDIT specimen were characterized by means of classical mechanical tests. A summary of the results is presented in tables 3 and 4 for concrete and steel respectively.

3.1.2. Deterministic mechanical models and calibration

Description. The geometry of the BANDIT specimen has allowed to consider three different mechanical models, all of them based upon the use of the FEM. Three FE strategies were used to assess the dynamic response of the specimen. Each of them is characterized by a given FE mesh. The FE meshes are shown in

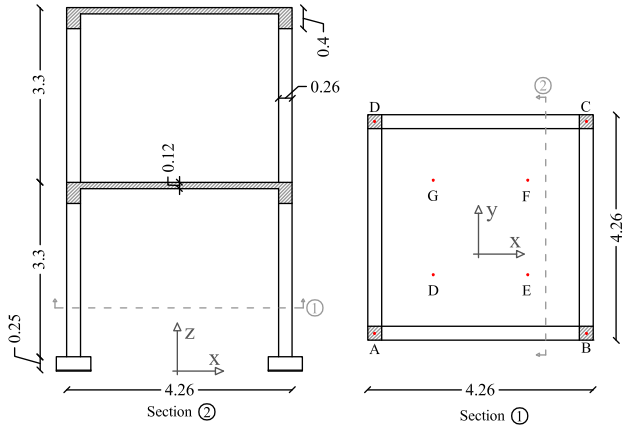

Figure 2: Geometry and control points of the BANDIT specimen - dimensions in meters.

Bar type	Young modulus (MPa)	Poisson ratio (-)	Yield stress (MPa)	Ultimate stress (MPa)	Density ($kg.m^{-3}$)
HA10	210000	0.3	513	585	7800
HA14	210000	0.3	526	616	7800

Table 4: Results from the mechanical test to characterize steel - BANDIT.

figures 3. In figure 3a, one can observe that multifibers Timoshenko's beam FE have been used [37, 22, 38]. This assessment approach is usually recognized as a reasonable trade-off between well-known beam FEs based approaches, which can include constitutive laws formulated in terms of stresses and strains. The computational time-consumption is lower than the one used by two-dimensional or three-dimensional approaches. In addition, it is applicable to describe the behaviour of beam-column structures. In figures 3b and 3c, classical two-dimensional[1] and three-dimensional FE meshes can be recognized. In the following, the aforementioned mechanical models are referred to 1D, 2D and 3D respectively. To avoid any misunderstanding, the latter labels have been defined with respect to the dimensional nature of the constitutive laws used in each case (1D in case of the multifiber approach, 2D in case of both plane stress and multilayer shell models and 3D in case of a full three-dimensional approach). For all the approaches, the steel reinforcing bars were meshed by fibers (in case of the 1D model) or by truss FEs (in case of the 2D and 3D models). The constitutive laws used to describe the mechanical behaviour of concrete and steel are based upon continuum damage mechanics [39] and plasticity theory [40] respectively. The main effects taken into account by the concrete constitutive law are the asymmetry between the softening behaviours in tension and in compression and the so-called unilateral effect [41] which is crucial when dealing with cyclic loadings. The steel/concrete interface is assumed to be perfect: a full load transfer between the steel and the surrounding concrete is allowed. In order to be able to compare the numerical results, the same constitutive laws were adopted for all the modelling strategies. The material parameters were identified from the results of the mechanical tests conducted (see tables 3 and 4) to characterize the elastic modulus, the thresholds and the hardening parameters of concrete and steel. In order to represent the contribution of the dissipated energy not taken into account by the constitutive laws and to avoid numerical issues mainly related to strain localization, a viscous damping model has been included in the numerical model. The well-known Rayleigh viscous damping model has been considered [42], leading to a viscous damping matrix proportional to both the initial stiffness (without updating) and the mass matrix. The parameters of the Rayleigh's damping model have been computed at each deterministic analysis from the two first initial eigenfrequencies of the RC specimen.

[1]The two-dimensional model is considered under the plane stress assumption.

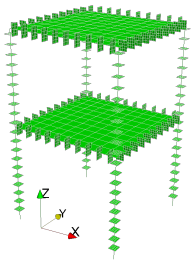

(a) Multifiber Timoshenko's beams.

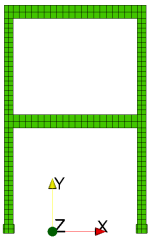

(b) Two-dimensional finite elements.

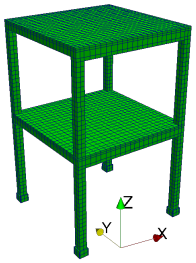

(c) Three-dimensional finite elements.

Figure 3: FE meshes used in the assessment approaches considered in case of the BANDIT specimen.

Model	Direction	Exp. eigenfrequency (Hz)	Num. eigenfrequency (Hz)	Gap (%)	First mode-shape
1D	X	1.9	1.9	≈0	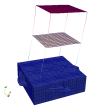
	Y	2.1	2.0	4	
2D	X	1.9	1.9	≈0	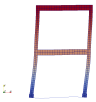
	Y	2.1	N/A	N/A	
3D	X	1.9	1.9	≈0	
	Y	2.1	2.0	4	

Table 5: Comparison between the measured eigenfrequencies and the computed values - BANDIT specimen - directions defined according to figure 2.

A mean damping ratio equal to 2% was chosen, which is an ordinary value when non linear constitutive laws are considered [43, 44, 45] . The nonlinear dynamic problem has been solved with the finite element software CAST3M [46], using a Newmarks time integration scheme the numerical parameters of which have been set to ensure unconditional stability (constant average acceleration). In addition, the time step is equal to 9.76 10^{-4} s and the convergence criterion (based on the norm of the residue vector) is equal to 10-4.

Calibration. After identifying the material parameters of each modelling strategies, a set of modal analyses has been performed to check if the first eigenfrequencies related to the models are in accordance with the ones measured. Then, to describe the experimental conditions, a model of the shaking table has been included for the calibration process. In this way, local flexibility at the interface between the specimen and the shaking table upper plate could be taken into account. The results are shown in table 5.

3.2. SMART 2013 experiment as a shearwall-based structure

3.2.1. Experimental setup

The RC specimen is a scaled model of a simplified half part of a nuclear electrical building. It has been prepared to reproduce the geometrical, physical and dynamical characteristics of a part of the real building. The RC specimen was designed according to the current French design rules to be considered when dealing with a nuclear building [43]. The design spectrum considered is shown in figure 4a. The design spectrum

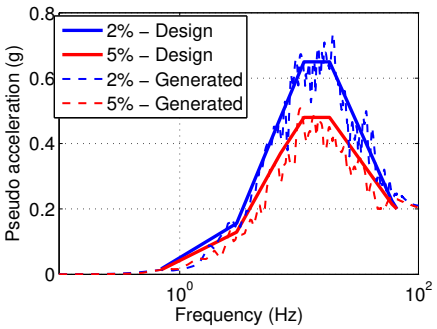

(a) Design spectrum for two damping ratios.

(b) Picture of the SMART 2013 specimen.

Figure 4: Design spectrum and picture of the SMART 2013 specimen.

is a simplified (linear segments) envelop of a seismic scenario corresponding to a magnitude of 5.5 recorded at 10 km of the fault plane. The Peak Ground Acceleration (PGA) is 0.2 g. Synthetic accelerograms were generated from the design spectrum and the corresponding acceleration response spectra are compared to the design spectra in figure 4a. A detailed description of the generation technique used can be found in [47]. A satisfactory agreement between the design spectra and the response spectra derived from synthetic signals can be pointed out. The accelerograms considered for the seismic loading is shown in appendix C.

The geometry of the RC specimen was defined in order to meet the following conditions: (i) the specimen should have an asymmetric shape to ensure significant torsional effects during the loading and (ii) the first eigenfrequencies should be in the range 4-10 Hz to ensure that significant damage appears and that the specimen is representative of existing nuclear buildings currently operated in France. A picture of the test specimen is exposed in figure 4b. It is composed of nine structural elements: one foundation, three shear walls (referenced as shear wall # 1 to # 4 in the in-plane view of the formwork drawings presented in figure 5), three slabs, three beams and one column. In order to avoid any potential differential displacements, a new anchorage and foundation design was considered with respect to the former SMART 2008 specimen. The continuous RC footing is 650 mm wide and 250 mm high; it is bolted on 34 anchoring points in a 20-mm-thick steel plate; planarity defaults are mitigated by means of a mortar layer against the steel plate which is fastened to the shaking table. Uniformly distributed additional masses are clamped on the mock-up slabs (apart from on the RC beams) to ensure the condition related to the similitude rule. The total mass of the RC specimen is then equal to 45.69 tons. Slabs are kept elastic as only minor cracking phenomena where observed during the experimental tests. The constitutive materials were characterized by means of

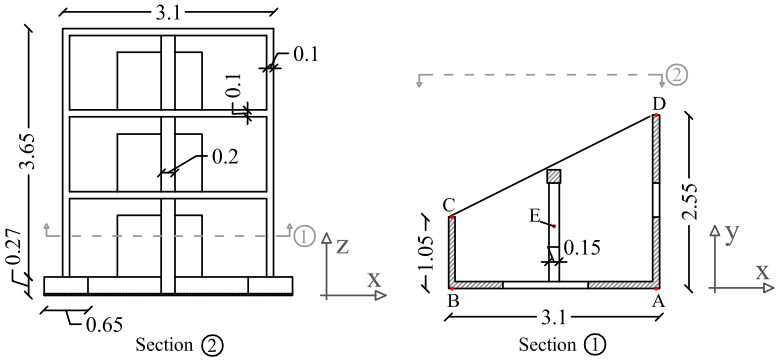

Figure 5: Geometry and control points of the SMART 2013 specimen - dimensions in meters.

Element	Young modulus (MPa)	Poisson ratio (-)	Compressive strength (MPa)	Tensile strenght (MPa)	Density ($kg.m^{-3}$)
Foundation	25400	0.17	43.3	3.45	2300
Shear wall - floor # 1	28700	0.19	41.7	3.15	2300
Shear wall - floor # 2	25700	0.19	35.5	2.70	2300
Shear wall - lloor # 3	29500	0.18	46.6	4.00	2300
Slab - floor #1	28200	0.18	41.1	3.25	2300
Slab - floor #2	24700	0.17	36.8	3.35	2300
Slab - floor #3	24400	0.18	37.8	3.40	2300
Column	25400	0.17	43.3	3.45	2300

Table 6: Results from the mechanical test to characterize concrete - SMART 2013.

Bar type	Young modulus (MPa)	Poisson ratio (-)	Yield stress (MPa)	Ultimate stress (MPa)	Density ($kg.m^{-3}$)
HA6	252666	0.3	505	565	7800
HA8	250166	0.3	500	571	7800

Table 7: Results from the mechanical test to characterize steel - SMART 2013.

classical mechanical tests. A summary of the results is presented in tables 6 and 7 for concrete and steel respectively.

3.2.2. Deterministic mechanical models and calibration

Description. According to the objectives of the SMART 2013 project, the specimen was designed to ensure that significant torsional effects will appear when subjected to a dynamic loading. Therefore, the SMART 2013 specimen is regular in elevation and irregular in-plane. In addition, it must be mentioned that despite the fact that some authors have successfully demonstrated the ability of these elements to describe the global response of wall-based structures [38], this strategy is still not in the common engineering practice. For the aforementioned reasons, 1D modelling strategy has not been considered to describe the behaviour of the SMART 2013 specimen. Thus, 2D and 3D modelling strategies were used. The FE meshes are presented in figures 6. In figure 6a, it can be observed that two-dimensional multilayer shell FEs have

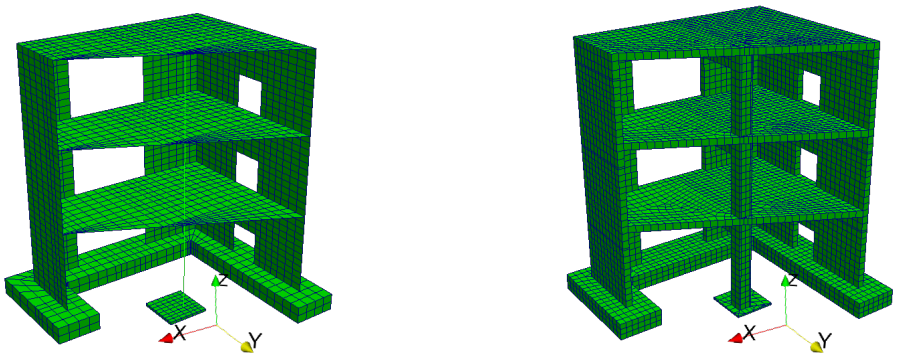

(a) Two-dimensional finite elements (b) Three-dimensional finite elements

Figure 6: FE meshes used in the assessment approaches considered in case of the SMART 2013 specimen.

been used for all the structural elements of the SMART 2013 specimen excepted for the foundation. This

Model	Direction	Exp. eigen-frequency (Hz)	Num. eigen-frequency (Hz)	Gap (%)	First mode-shape
2D	X	6.3	6.3	≈0	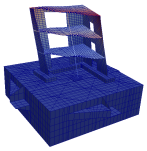
	Y	7.9	8.1	2.5	
	Z	16.5	19.6	18.7	
3D	X	6.3	6.4	1.5	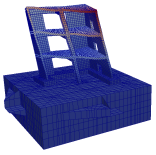
	Y	7.9	8.2	3.8	
	Z	16.5	19.8	20	

Table 8: Comparison between the measured eigenfrequencies and the computed values - SMART 2013 specimen - directions defined according to figure 5.

latter element has been meshed with three-dimensional FEs. The column is described by Timoshenko's beam elements. Indeed, because this structural element does not have critical structural function, a rough description of its behaviour has been judged as sufficient. In figure 6b, the full three-dimensional mesh used in the 3D modelling strategy is shown. The constitutive laws used to represent the mechanical behaviour of concrete and steel are the same as ones used in case of the BANDIT specimen (see [39, 40] for concrete and steel respectively). It can be noticed that the slabs are considered elastic for the same reasons as the ones exposed in case of the BANDIT case-study. In addition, the steel/concrete interface has also been considered as being perfect. The material parameters of each constitutive laws were identified according to the results of the mechanical tests performed on concrete and steel specimens (see tables 6 and 7). It can be noticed that the spatial distribution of the concrete properties has been taken into account in the identification process. Similarly to the case of BANDIT specimen, additional dissipation has been included in the model by considering the Rayleigh damping model. The damping matrix calibration procedure and the methodology used to solve the dynamic non linear problem are the same as the ones exposed in section 3.1.2. The viscous damping ratio considered in case of SMART 2013 is equal to 2.8%.

Calibration. Similarly to the case of the BANDIT specimen, a set of modal analyses has been performed to check the calibration of the modelling strategies. The results are shown in table 8. One can notice that, for the 2D and 3D modelling approaches, the two first eigenmodes are described in a satisfactory way. On the contrary, for both approaches, the last eigenmode is not well captured. To understand this gap, it is of interest to mention that the modal properties (eigenfrequencies, modal damping ratios and modeshapes) are experimentally identified by the operational modal analysis [48, 49, 50] realized on the basis of the structural responses measured during the initial white noise excitation. This approach provides estimations of the modal properties of the dynamic system composed of the structure, the shaking table and the hydraulic system used to supply the actuators with the necessary power. However, the numerical modal analysis aims to solve an eigenvalue problem which does not take the hydraulic system into account. Therefore, both analyses provide estimations of modal properties that are not exactly related to the same structural system. This point might explain the differences observed between the numerical and the experimental values of the eigenfrequencies. However, it is important to notice that no adjustment of the material parameters has been made; the numerical eigenfrequencies and modeshapes are obtained by inputting the measured material parameters.

3.3. Constitutive laws and material parameters

First, for all the modeling strategies considered in this paper, the constitutive laws used not only for steel but also for concrete are formulated in the same way. In case of steel [40], the constitutive law is always one-dimensional. In case of concrete [39], the only difference are related to the kinematics constraints (shape of the strain and stress matrices) to take into account the formulation of the finite elements themselves. More precisely:

1. in case of the multifiber framework, one-dimensional versions of the original constitutive laws are derived;
2. in case of the plane stress-like frameworks (either multilayer shells or more classical plane stress), the plane stress condition has to be fulfilled and two-dimensional version of the original constitutive laws are derived;
3. in case of the full three-dimensional framework (solid finite elements), the original version of the constitutive law is used.

Therefore, the number of parameters used in each case and the complexity of the constitutive laws are the same for all the case-studies. From a physical point of view, the concrete constitutive law takes into account three dissipative mechanisms: (i) softening in tension, which is modelling by continuous damage in order to describe cracking; (ii) hysteretic effects, which are associated with friction occurring between the cracking surfaces; and (iii) the unilateral effect, which is physically explained the fact that crack opened in tension close in compression. In this case, the elastic stiffness if recovered while damage is not null. As it is often the case with damage based constitutive laws, the fracture energy influences the shape of the post-peak response of the laws in terms of stresses and strains. The damage law is of exponential type and depends on a parameter that can be linked with the cracking energy itself. The mean value has been computed from the model code 2010 recommendations.

Second, regarding the way of the material parameters considered as being random are formulated, it is not the same for all the parameters. In case of the concrete Young modulus, the tensile strength and the yield stress, these parameters are used in the constitutive laws straightforwardly (one elastic parameter and two thresholds). Regarding the cracking energy, this parameter is actually expressed as a function of (i) other (unphysical) parameters (which quite classical for concrete models) and (ii) a characteristic length linked with the mesh size. In case of the damping ratio, this parameter is not linked with constitutive laws but is linked with the formulation of the balance equations expressed within a dynamic context. Despite the fact the aforementioned parameters does not act on the same way on the results, the way of acting is similar for all the case-studies considered.

Last, the loading direction has not been assumed. It has been defined and applied to the structural model in a consistent way with respect to the experiment. So, the degradation processes should be influenced by this parameter but the present study does not allows to quantify it. In addition, when it comes to the directional effects, it is important to distinguish two aspects: (i) the directional effects at the member scale that appear due to the strong asymmetry (especially in case of SMART 2013 case study) and (ii) the directional effect taken into account at the constitutive law level. In case of the first one, because it is purely geometric, no direct connection with the constitutive laws can be made. In that sense, the constitutive laws do not account for specific mechanisms in connection with it. The fact that the geometry of the case studies is described allows for taking into account this effect. In case of the second aspect, all the constitutive laws used allow to describe the response of a representative volume element (RVE) which is assumed to be isotropic. Therefore, no directional effects are taken into account at the constitutive laws level.

3.4. Shaking table modelling: accurate application of the loading conditions

In order to ensure an accurate control of the boundary conditions, the shaking table has also been included in the structural models of both specimens. It is composed only of multilayer shell finite elements, since the shaking table can be seen as an assembly of shells and plates. A detailed description of the

shaking table model can be found in [51]. Indeed, the way of controlling the boundary conditions is essential to making an accurate description of the dynamic behaviour of a specimen during a shaking table test. Since specific attention has been paid to monitoring the displacement and acceleration time histories at the junction between the actuators and the shaking table, benefits could be taken from this information. In order to accurately take into account the complex kinematics of the dynamic system, seismic loading has been applied by prescribing the displacement time histories at each connection point between the eight actuators and the shaking table. The non linear dynamic problems have been solved in the absolute reference frame. Once the problems solved, the acceleration time histories monitored at the bottom of the foundation were compared to the computed ones in order to check the correct application of the seismic loading. Thus,

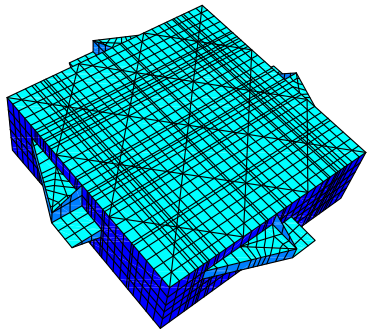

Figure 7: FE mesh of the AZALEE shaking table.

available information related to the displacement time evolution of the actuators was used to control the loading in case of the BANDIT and SMART 2013 specimens. More precisely, the BANDIT specimen was subjected to one-dimensional seismic loading. The design level has been considered. The SMART 2013 specimen has been subjected to a bi-dimensional loading, in accordance with the experimental setting. In both cases, the loading corresponded to the design level. In this way, even though both structures are different, the intensity of the loading applied could be considered as relatively similar.

4. Results and discussion

In this section, the results obtained from the probabilistic analysis are presented. Firstly, the statistical robustness of the analysis is assessed by studying the convergence of the variance related to the selected EDPs. These preliminary results are of primary importance to demonstrate the relevancy of the statistical treatments presented. Secondly, a focus on the sensitivity of specific EDPs is made. Lastly, a summary of the results including the structural typology and the type of modelling strategy is presented and discussed.

4.1. Statistical convergence

The statistical convergence is assessed by computing the gap between two variance estimations as a function of the sample number. This computation has been carried out considering each structural typology, modelling strategy and the selected EDP. Given a structural typology and assessment technique, the following quantity has been computed for all the selected EDPs.

$$\Delta_i(n) = \frac{\boldsymbol{Var}(\boldsymbol{y}_i)_{n+1} - \boldsymbol{Var}(\boldsymbol{y}_i)_n}{\underset{0 \leq p \leq n}{\boldsymbol{max}} \left(\boldsymbol{Var}(\boldsymbol{y}_i)_p\right)} \tag{3}$$

and:

$$\boldsymbol{Var}(\boldsymbol{y}_i) = \frac{\sum_{j=1}^{n} \left(y_i^j - \mu(\boldsymbol{y}_i)\right)^2}{n-1} \tag{4}$$

where $\Delta_i(n)$ stands for the convergence index for n realizations of the i^{th} EDP, $\mu(\boldsymbol{y}_i)$ is the statistical mean. In case of the BANDIT specimen, the results are shown in figures 8. For all the EDPs, the convergence is reached after 50 samples. It is interesting to emphasize on the fact that for all the EDPs, excepted the AMPR, the 3D modelling strategy exhibits the fastest convergence rate. The 1D strategy is the one which exhibits the lowest convergence rate. Regarding the SMART 2013 specimen, the results are shown in figures

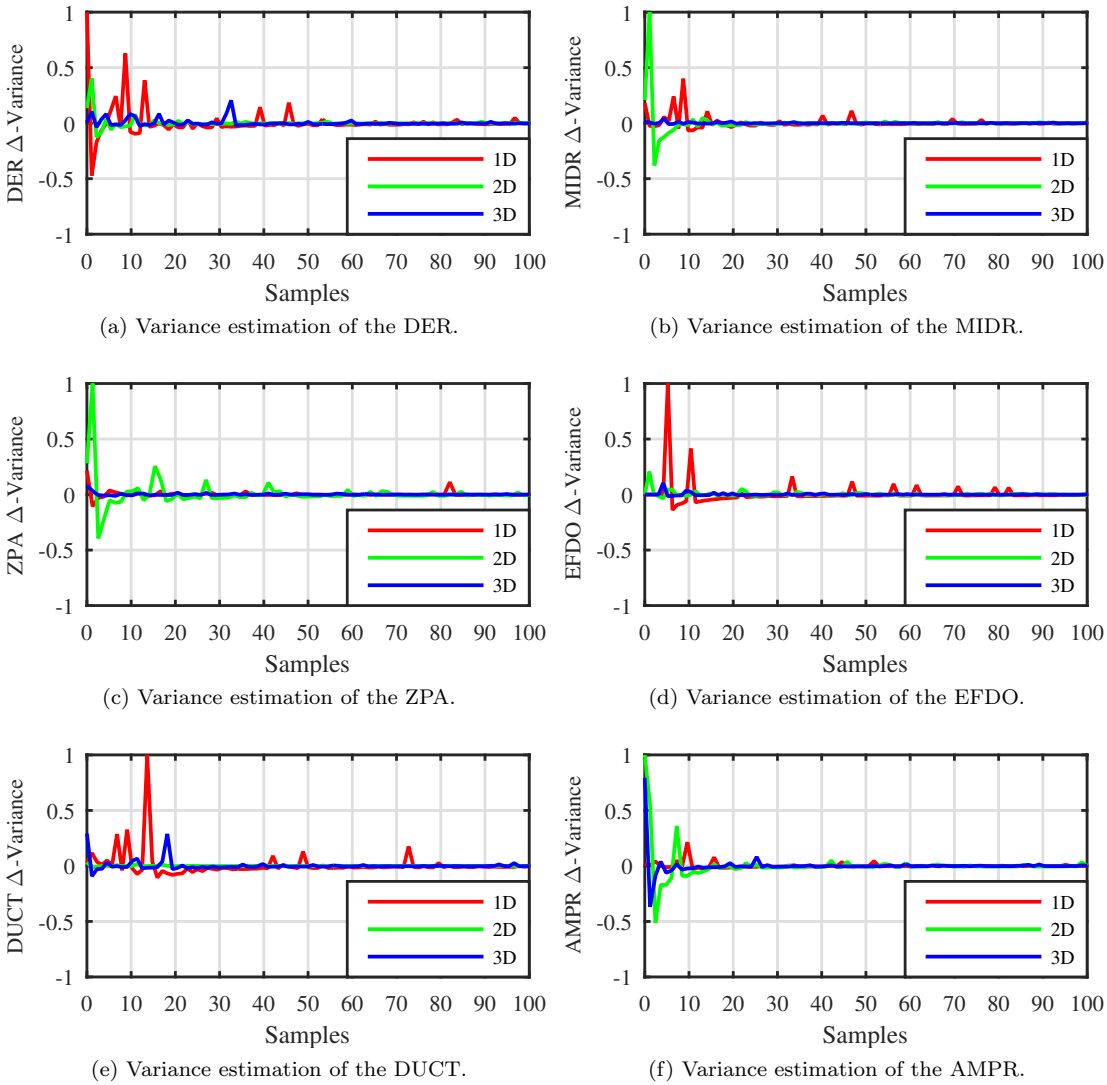

(a) Variance estimation of the DER.

(b) Variance estimation of the MIDR.

(c) Variance estimation of the ZPA.

(d) Variance estimation of the EFDO.

(e) Variance estimation of the DUCT.

(f) Variance estimation of the AMPR.

Figure 8: Consecutive gaps between two variance estimations - BANDIT.

9. Similarly to the case of BANDIT specimen, the convergence is reached after 50 samples. However, the trend between the 2D and 3D modelling approaches is not the same. Indeed, the 3D assessment approach leads to the lowest convergence rate for almost all the EDPs, whereas the 2D modelling strategy exhibits a better convergence rate.

4.2. Focus on specific EDPs

In this section, a focus is made on three specific EDPs: the DER, the MIDR and the ZPA. In this way, an energy-based quantity, a displacement-based quantity and an spectral-based quantity are analysed.

4.2.1. Sensitivity of the DER

The time evolution of the DER are shown in figures 10 and 11 for the BANDIT and the SMART 2013 specimens respectively. Regarding the case of the BANDIT specimen, the general trend observed for the 2D and 3D modelling strategies is consistent. In addition, it can be noticed that the results obtained by the 3D assessment approach are highly sensitive to the material parameters' uncertainties, especially from 0 to 5 s. Regarding the case of the SMART 2013 specimen, the mean time evolution and the confidence interval of the DER computing from the 2D approach is in accordance with the one resulting from the 3D strategy. However, it is interesting to notice that the DER is more sensitive to the parameter uncertainties in case of the SMART 2013 structure than in case of the BANDIT structure. The characteristics of the material parameter uncertainties being the same for both structures, it seems clear that the structural typology affects the uncertainty propagation. More precisely, it is important to keep in mind that the 2D modelling refers to the model for which the plane stress condition should be satisfied: this means (i) classical plane stress model and (ii) shell models. In the first case, it is obvious that out-of-plane effects are not taken into account. In the second case, shell based models may roughly represent out-of-plane effects [52]. Given this observation, the fact of describing in a refine way these effects may lead to compensations which would result in increasing the sensitivity of structural responses. This is a first assumption for which further investigations to be confirmed. In addition, for both case-studies, it is interesting to notice that during the first seconds, values of DER close to 1 are obtained (see figures 10 and 11. This may be explained the fact that in the elastic phase all the input energy is equal to the kinetic energy, as we do not have any dissipation through damage or viscous damping. At the initial step, the kinetic and the damping energies tends to be equal to zero. Therefore, the DER is close to 1.

4.2.2. Sensitivity of the MIDR

Among the EDPs selected in this work, the MIDR is one of the most used EDP in the engineering community. In many standards [53, 36, 54, 55], the assessment of limit states requires an estimation of the MIDR. The time evolution of the MIDR are shown in figures 12 and 13, for the BANDIT and SMART 2013 specimens respectively. Regarding the case of the BANDIT specimen, the width of the confidence interval is almost the same for all the used modelling strategies. In addition, one can notice that the results obtained with the 2D strategy and shown in figure 12b exhibit a higher frequency content than the other ones. This may be explained by the fact that the 2D assessment approach, by nature, does not take into account out-of-plane effects. These effects might have appeared in the shaking table experiment. Not taking them into account may lead to a stiffer structural response. Regarding the case of SMART 2013 specimen, the width of the confidence interval is higher than in case of the BANDIT specimen. This trend is similar to the one observed in figures 10 and 11. A similar reason to explain this observation may be invoked.

4.2.3. Sensitivity of the ZPA

The ZPA is used in many conventional assessment methodologies. For instance, the pseudo-static method [56, 57] is classically used as a preliminary analysis to assess structures or equipment. One of the inputs of the method is the equivalent pseudo-static force, which is computed as the product between a mass term and the ZPA. The time evolutions of the ZPA are shown in figures 14 and 15 for the BANDIT and SMART 2013 specimens respectively. Regarding the BANDIT specimen, figures 14a, 14b and 14c show similar trends: the mean responses are consistent as well as the width of the confidence intervals. On the contrary, the results related to the SMART 2013 specimen show a higher sensitivity to the material parameter uncertainties, especially in case of the 3D modelling approach.

4.3. Sensitivity matrix

In order to quantify the sensitivity of all the selected EDPs, their associated COV were estimated. The results are shown in figures 16a and 16b for the BANDIT and the SMART 2013 specimens respectively. For both cases, one of the most sensitive EDP is the ZPA even though it should be noted that the range of variation of this index is not the same for both cases. On the other hand, for both cases, the least sensitive index is the AMPR. According to the definition of the AMPR, this observation means that the effects of the

uncertainties on the ZPA are somehow balanced by the variations of the maximum spectral acceleration. In addition, results clearly show that the EDPs computed in case of the SMART 2013 specimen are more sensitive, than the ones computed in case of the BANDIT specimen. This trend is consistent with the ones identified in the analysis of specific EDPs, previously exposed. regarding the effect of the assessment methodology, a general trend is not easy to identify. In case of the BANDIT specimen, the 1D modelling strategy leads to the most sensitive EDPs, whereas in case of the SMART 2013 specimen, it is the 3D approach. However, in both cases, the 2D modelling approach appears as being less sensitive to the material parameter uncertainties than the other ones.

5. Conclusions, recommendation and outlook

In this study, the effects of material parameter uncertainties on selected EDPs are analyzed and quantified, as a function of the structural typology and the assessment methodology. In this regard, two shaking table experiments have been selected, namely the BANDIT and SMART 2013 experimental campaigns. Even though many studies have allowed to establish a consensus on the fact that uncertainties on the seismic input ground motions higher than the ones on material parameters, the consequences of considering them random variables were never fully analyzed. To this end, the seismic input ground motion was assumed to be deterministic. In this way, conclusions on the effects of material parameter uncertainties could be drawn. Despite the fact that only one structure for each structural typology has been analyzed in this study, first trends could be identified. In accordance with the results presented in this paper, the following conclusions have been reached:

- a shear-wall-based structure exhibit more sensitive responses than a beam-column one;
- 1D and 3D modelling approaches lead to structural response which are more sensitive than the 2D modelling approach;
- the amplification ratio is the least sensitive EDP, whereas the ZPA is the most sensitive one.

As first recommendations for the structural engineering community, the results of this study can be expressed in a pragmatic manner. Figure 17 shows a sensitivity matrix for the two structural typologies and for all the considered assessment methods. This matrix should help engineers, especially when choosing the EDP to better apprehend the sensitivity of the structural responses. More precisely, let us assume that a fragility curve is represented by a median capacity A_m and a standard deviation β. If engineers use a given modeling strategy and EDP(s) that is(are) not sensitive to the uncertainties related to the input parameters, the resulting uncertainties level should be decreased. Therefore, the confidence interval associated to the fragility curve should be narrower and the median capacity should be lower (if we considered that the slope of the fragility curve at $P_f = 0.5$ is mainly driven by the standard deviation). The results reported in this paper allowed for identifying trends in order to assess the sensitivity of specific EDPs with respect to the uncertainties related of the input material parameters, for different modeling strategies and structural typologies. However, this study has limitations regarding several aspects which would deserve to be further investigated. Among theses limitations, three keypoints can be mentioned: (i) the influence of the seismic signal itself on the covariance matrix, (ii) the influence of the uncertainties related to each material parameter and (iii) the influence of the seismic loading directions. Especially, regarding the second aspect, specific well-known indices [58] could be estimated to bring some answers.

Acknowledgements

The work carried out under the SINAPS@ project has benefited from French funding managed by the National Research Agency under the program Future Investments (SINAPS@ grant No. ANR-11-RSNR-0022). This work has also been supported by the SEISM Institute (http://www.institut-seism.fr).

Appendix A: realizations of the input variables - BANDIT case-study.

Appendix B: realizations of the input variables - SMART 2013 case-study.

Appendix C: input accelerograms used for BANDIT and SMART 2013.

[1] EPRI, Seismic probabilistic risk assessment implementation guide, Tech. rep., Electric Power Research Institute EPRI, Palo Alto, CA, report 1002989 (2013).
[2] EPRI, Methodology for developing seismic fragilities, Tech. rep., Electric Power Research Institute EPRI, Palo Alto, CA, report TR-103959 (1994).
[3] I. Zentner, M. Gündel, N. Bonfils, Fragility analysis methods: Review of existing approaches and application, Nuclear Engineering and Design 323 (2017) 245–258.
[4] M. Shinozuka, M. Q. Feng, J. Lee, T. Naganuma, Statistical analysis of fragility curves, Journal of engineering mechanics 126 (12) (2000) 1224–1231.
[5] D. Lallemant, A. Kiremidjian, H. Burton, Statistical procedures for developing earthquake damage fragility curves, Earthquake Engineering & Structural Dynamics 44 (9) (2015) 1373–1389.
[6] I. Gidaris, A. A. Taflanidis, G. P. Mavroeidis, Kriging metamodeling in seismic risk assessment based on stochastic ground motion models, Earthquake Engineering & Structural Dynamics 44 (14) (2015) 2377–2399.
[7] C. Mai, K. Konakli, B. Sudret, Seismic fragility curves for structures using non-parametric representations, Frontiers of Structural and Civil Engineering 11 (2) (2017) 169–186.
[8] R. P. Kennedy, C. Cornell, R. Campbell, S. Kaplan, H. Perla, Probabilistic seismic safety study of an existing nuclear power plant, Nuclear Engineering and Design 59 (2) (1980) 315–338.
[9] H. Y. Noh, D. Lallemant, A. S. Kiremidjian, Development of empirical and analytical fragility functions using kernel smoothing methods, Earthquake Engineering & Structural Dynamics 44 (8) (2015) 1163–1180.
[10] M. J. Fox, T. J. Sullivan, K. Beyer, Evaluation of seismic assessment procedures for determining deformation demands in rc wall buildings, Earthquakes and Structures 9 (EPFL-ARTICLE-213147) (2015) 911–936.
[11] H. Xu, P. Gardoni, Probabilistic capacity and seismic demand models and fragility estimates for reinforced concrete buildings based on three-dimensional analyses, Engineering Structures 112 (2016) 200–214.
[12] J. M. O'Connor, B. Ellingwood, Reliability of nonlinear structures with seismic loading, Journal of Structural Engineering 113 (5) (1987) 1011–1028.
[13] P. Gehl, D. M. Seyedi, J. Douglas, Vector-valued fragility functions for seismic risk evaluation, Bulletin of Earthquake Engineering 11 (2) (2013) 365–384.
[14] D. Seyedi, P. Gehl, J. Douglas, L. Davenne, N. Mezher, S. Ghavamian, Development of seismic fragility surfaces for reinforced concrete buildings by means of nonlinear time-history analysis, Earthquake Engineering & Structural Dynamics 39 (1) (2010) 91–108.
[15] Z. Wang, I. Zentner, E. Zio, A bayesian framework for estimating fragility curves based on seismic damage data and numerical simulations by adaptive neural networks, Nuclear Engineering and Design 338 (2018) 232–246.
[16] O.-S. Kwon, A. Elnashai, The effect of material and ground motion uncertainty on the seismic vulnerability curves of rc structure, Engineering structures 28 (2) (2006) 289–303.
[17] F. Lopez-Caballero, A. Modaressi-Farahmand-Razavi, Assessment of variability and uncertainties effects on the seismic response of a liquefiable soil profile, Soil Dynamics and Earthquake Engineering 30 (7) (2010) 600–613.
[18] C. A. Cornell, F. Jalayer, R. O. Hamburger, D. A. Foutch, Probabilistic basis for 2000 sac federal emergency management agency steel moment frame guidelines, Journal of structural engineering 128 (4) (2002) 526–533.
[19] P. Beverly, fib model code for concrete structures 2010, Ernst & John, 2013.
[20] M. Rosenblatt, Remarks on a multivariate transformation, The annals of mathematical statistics 23 (3) (1952) 470–472.
[21] R. Lebrun, A. Dutfoy, Do rosenblatt and nataf isoprobabilistic transformations really differ?, Probabilistic Engineering Mechanics 24 (4) (2009) 577–584.
[22] E. Spacone, F. C. Filippou, F. F. Taucer, Fibre beam–column model for non-linear analysis of r/c frames: Part i. formulation, Earthquake Engineering & Structural Dynamics 25 (7) (1996) 711–725.
[23] T. Belytschko, H. Stolarski, W. K. Liu, N. Carpenter, J. S. Ong, Stress projection for membrane and shear locking in shell finite elements, Computer Methods in Applied Mechanics and Engineering 51 (1-3) (1985) 221–258.
[24] O. C. Zienkiewicz, R. L. Taylor, O. C. Zienkiewicz, R. L. Taylor, The finite element method, Vol. 36, McGraw-hill London, 1977.
[25] R. Y. Rubinstein, D. P. Kroese, Simulation and the Monte Carlo method, Vol. 10, John Wiley & Sons, 2016.
[26] K. A. Porter, An overview of peers performance-based earthquake engineering methodology, in: Proceedings of ninth international conference on applications of statistics and probability in civil engineering, 2003.
[27] J. Moehle, G. G. Deierlein, A framework methodology for performance-based earthquake engineering, in: 13th world conference on earthquake engineering, Vol. 679, 2004.
[28] B. Richard, P. Martinelli, F. Voldoire, T. Chaudat, S. Abouri, N. Bonfils, Smart 2008: Overview, synthesis and lessons learned from the international benchmark, Engineering Structures 106 (2016) 166–178.
[29] B. Richard, S. Cherubini, F. Voldoire, P.-E. Charbonnel, T. Chaudat, S. Abouri, N. Bonfils, Smart 2013: Experimental and numerical assessment of the dynamic behavior by shaking table tests of an asymmetrical reinforced concrete structure subjected to high intensity ground motions, Engineering Structures 109 (2016) 99–116.
[30] S. K. Ghosh, D. A. Fanella, Seismic and Wind Design of Concrete Buildings:(2000 IBC, ASCE 7-98, ACI 318-99), Kaplan AEC Engineering, 2003.
[31] R. Garcia, I. Hajirasouliha, M. Guadagnini, Y. Helal, Y. Jemaa, K. Pilakoutas, P. Mongabure, C. Chrysostomou, N. Kyriakides, A. Ilki, et al., Full-scale shaking table tests on a substandard rc building repaired and strengthened with post-tensioned metal straps, Journal of Earthquake Engineering 18 (2) (2014) 187–213.
[32] R. Garcia, I. Hajirasouliha, K. Pilakoutas, Y. Helal, Y. Jemaa, M. Guadagnini, M. Petkovski, P. Mongabure, M. A. Ciupala, N. Kyriakides, et al., Shake table tests on deficient rc buildings strengthened using post-tensioned metal straps, in: Seismic Evaluation and Rehabilitation of Structures, Springer, 2014, pp. 187–202.

[33] B. Richard, F. Voldoire, M. Fontan, J. Mazars, T. Chaudat, S. Abouri, N. Bonfils, Smart 2013: Lessons learned from the international benchmark about the seismic margin assessment of nuclear rc buildings, Engineering Structures 161 (2018) 207–222.

[34] P. Bisch, A. Coin, Seismic behaviour of slightly reinforced concrete walls: Experiments and theoretical conclusions, Bulletin of Earthquake Engineering 5 (1) (2007) 45–65.

[35] N. Ile, X.-H. Nguyen, P. Kotronis, J. Mazars, J. M. Reynouard, Shaking table tests of lightly rc walls: Numerical simulations, Journal of Earthquake Engineering 12 (6) (2008) 849–878.

[36] P. Code, Eurocode 8: Design of structures for earthquake resistance-part 1: general rules, seismic actions and rules for buildings, Brussels: European Committee for Standardization.

[37] J. Guedes, P. Pegon, A. Pinto, A fibre/timoshenko beam element in castem 2000. special publication nr. i. 94.31, applied mechanics unit, Institute for Safety Technology, Joint Research Centre, Commission of the European Communities, I-21020 ISPRA (VA), Italy.

[38] J. Mazars, P. Kotronis, F. Ragueneau, G. Casaux, Using multifiber beams to account for shear and torsion: Applications to concrete structural elements, Computer Methods in Applied Mechanics and Engineering 195 (52) (2006) 7264–7281.

[39] M. Vassaux, B. Richard, F. Ragueneau, A. Millard, Regularised crack behaviour effects on continuum modelling of quasi-brittle materials under cyclic loading, Engineering Fracture Mechanics 149 (2015) 18–36.

[40] M. Menegotto, P. E. Pinto, Slender rc compressed members in biaxial bending, Journal of the Structural Division 103 (3).

[41] C. La Borderie, Phénomènes unilatéraux dans un matériau endommageable: Modélisation et application à l'analyse de structures en béton., Ph.D. thesis, Paris 6 (1991).

[42] L. Rayleigh, On the pressure developed in a liquid during the collapse of a spherical cavity, Philosophical Magazine Series 6 (34) (1917) 94–98.

[43] O. Gupta, A. Lacoste, Prise en compte du risque sismique à la conception des ouvrages de génie civil dinstallations nucléaire de base à lexception des stockages à long terme des déchets radioactifs. guide de lautorité de sûreté nucléaire, Tech. rep., ASN/GUIDE/2/01. Autorité de Sûreté Nucléaire (2006).

[44] R. Crambuer, B. Richard, N. Ile, F. Ragueneau, Experimental characterization and modeling of energy dissipation in reinforced concrete beams subjected to cyclic loading, Engineering Structures 56 (2013) 919–934.

[45] T. Heitz, A. Le Maoult, B. Richard, C. Giry, F. Ragueneau, Dissipations in reinforced concrete components: Static and dynamic experimental identification strategy, Engineering Structures 163 (2018) 436–451.

[46] P. Verpeaux, T. Charras, A. Millard, Castem 2000: une approche moderne du calcul des structures, Calcul des structures et intelligence artificielle 2 (1988) 261–271.

[47] C. Pedron, Generation and characterization of synthetic signals: preliminary observations and developments, Tech. rep., DEN technical report, SEMT/EMSI/RT/98-022/A (1998).

[48] L. Zhang, R. Brincker, An overview of operational modal analysis: major development and issues, in: 1st international operational modal analysis conference, Aalborg Universitet, 2005, pp. 179–190.

[49] J. Brownjohn, F. Magalhaes, E. Caetano, A. Cunha, Ambient vibration re-testing and operational modal analysis of the humber bridge, Engineering Structures 32 (8) (2010) 2003–2018.

[50] A. Bajrić, J. Høgsberg, F. Rüdinger, Evaluation of damping estimates by automated operational modal analysis for offshore wind turbine tower vibrations, Renewable Energy 116 (2018) 153–163.

[51] A. Le Maoult, J.-C. Queval, R. Bairrao, Dynamic interaction between the shaking table and the specimen during seismic tests, in: Advances in Performance-Based Earthquake Engineering, Springer, 2010, pp. 431–440.

[52] T. J. Hughes, W. K. Liu, Nonlinear finite element analysis of shells: Part i. three-dimensional shells, Computer methods in applied mechanics and engineering 26 (3) (1981) 331–362.

[53] B. S. S. Council, Nehrp guidelines for the seismic rehabilitation of buildings (fema 273), Washington, DC: Federal Emergency Management Agency.

[54] B. S. S. Council, Nehrp recommended seismic provisions for new buildings and other structures (fema p-750), Washington, DC: Federal Emergency Management Agency.

[55] N. D. Lagaros, M. Fragiadakis, Evaluation of asce-41, atc-40 and n2 static pushover methods based on optimally designed buildings, Soil Dynamics and Earthquake Engineering 31 (1) (2011) 77–90.

[56] M. Karray, M. N. Hussien, M.-C. Delisle, C. Ledoux, Framework to assess the pseudo-static approach for the seismic stability of clayey slopes, Canadian Geotechnical Journal (ja).

[57] H. Mostafaei, M. S. Gilani, M. Ghaemian, A comparative study between pseudo-static and dynamic analyses on rock wedge stability of an arch dam, Civil Engineering Journal 4 (1) (2018) 179–187.

[58] B. Richard, L. Adelaide, C. Cremona, A. Orcesi, A methodology for robust updating of nonlinear structural models, Engineering structures 41 (2012) 356–372.

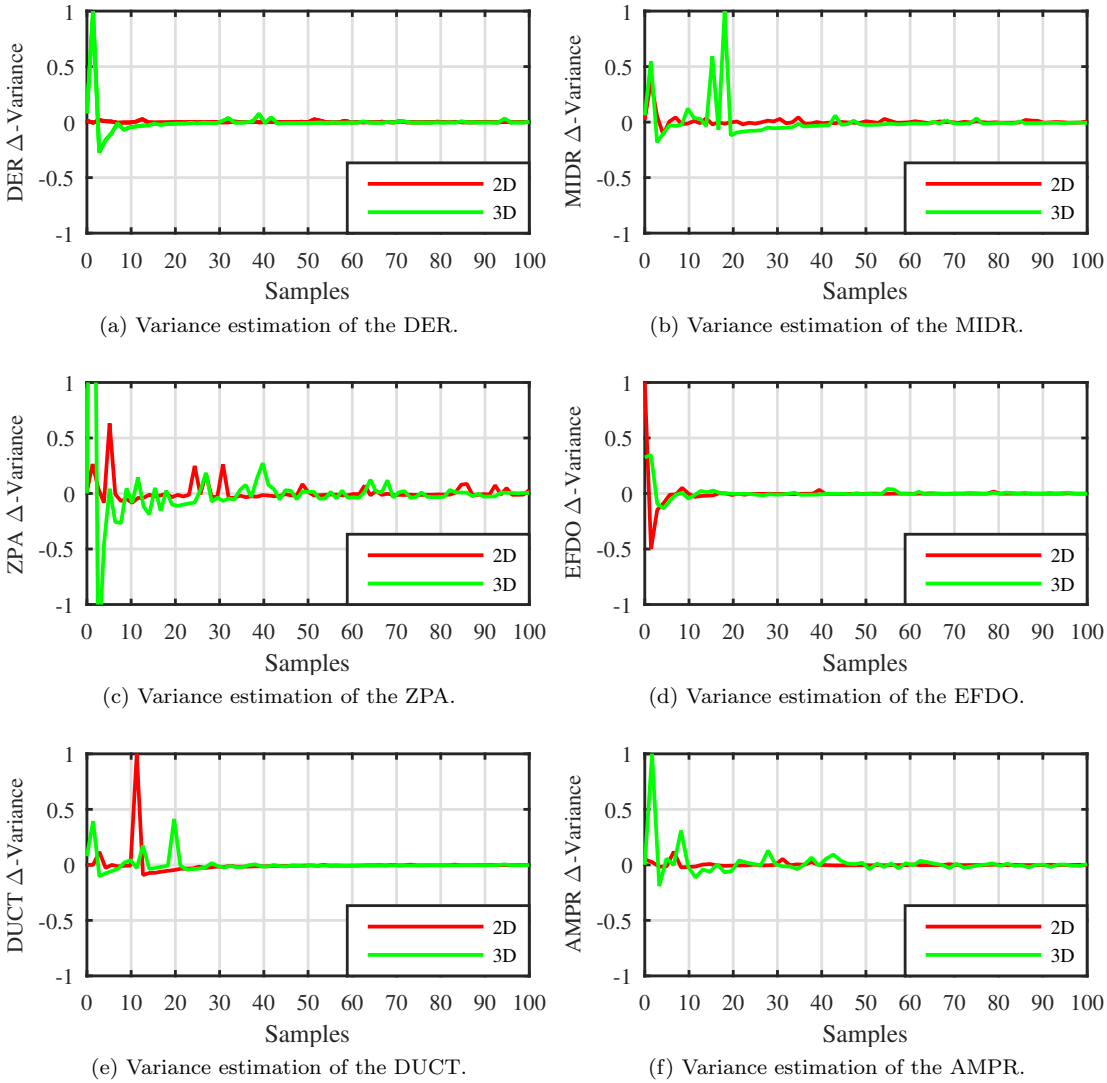

(a) Variance estimation of the DER.

(b) Variance estimation of the MIDR.

(c) Variance estimation of the ZPA.

(d) Variance estimation of the EFDO.

(e) Variance estimation of the DUCT.

(f) Variance estimation of the AMPR.

Figure 9: Consecutive gaps between two variance estimations - SMART 2013.

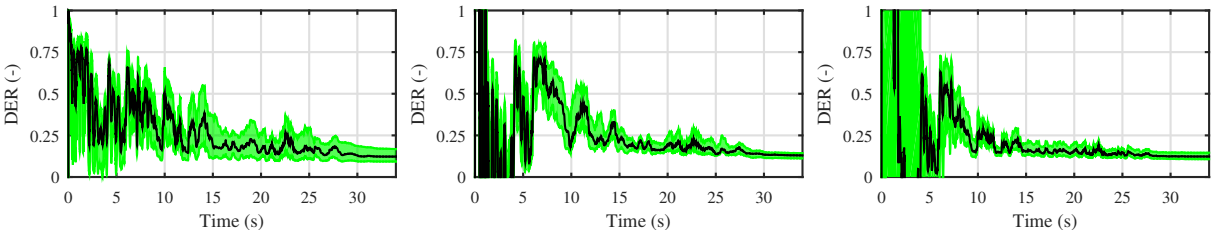

(a) 1D modelling strategy.

(b) 2D modelling strategy.

(c) 3D modelling strategy.

Figure 10: Time evolution of the DER - 90% confidence interval is depicted in green - BANDIT.

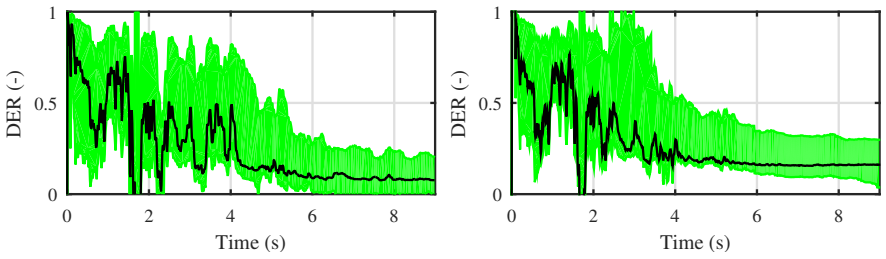

(a) 2D modelling strategy. (b) 3D modelling strategy.

Figure 11: Time evolution of the DER - 90% confidence interval is depicted in green - SMART 2013.

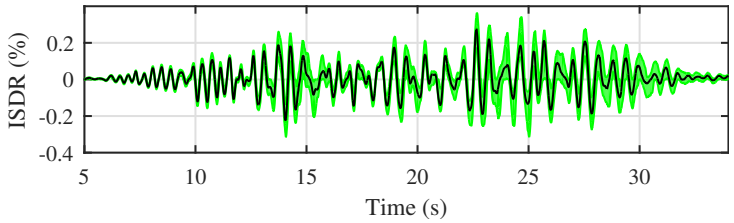

(a) 1D modelling strategy.

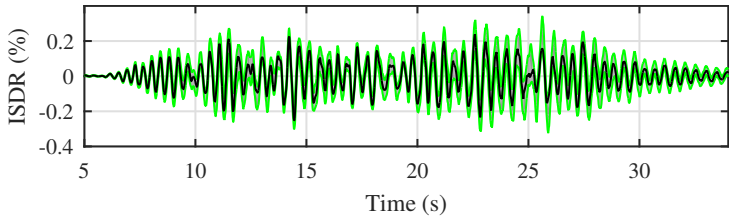

(b) 2D modelling strategy.

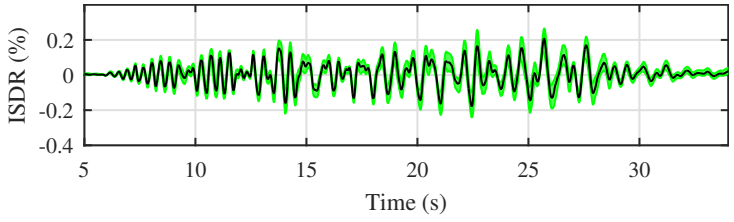

(c) 3D modelling strategy.

Figure 12: Time evolution of the MIDR - 90% confidence interval is depicted in green - BANDIT.

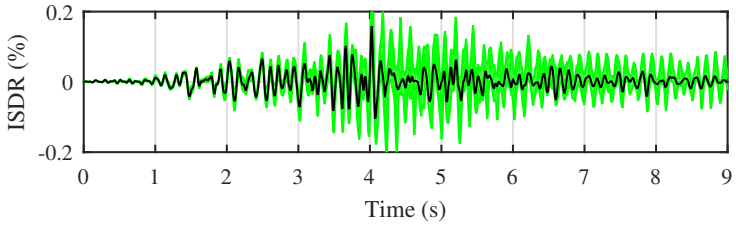

(a) 2D modelling strategy.

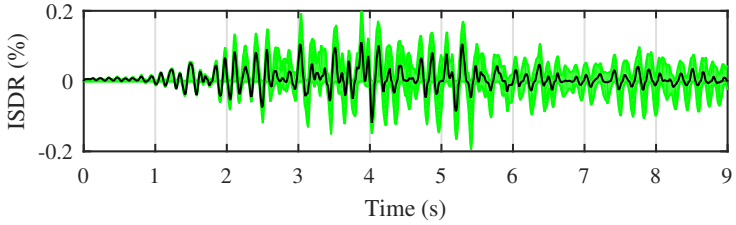

(b) 3D modelling strategy.

Figure 13: Time evolution of the MIDR - 90% confidence interval is depicted in green - SMART 2013.

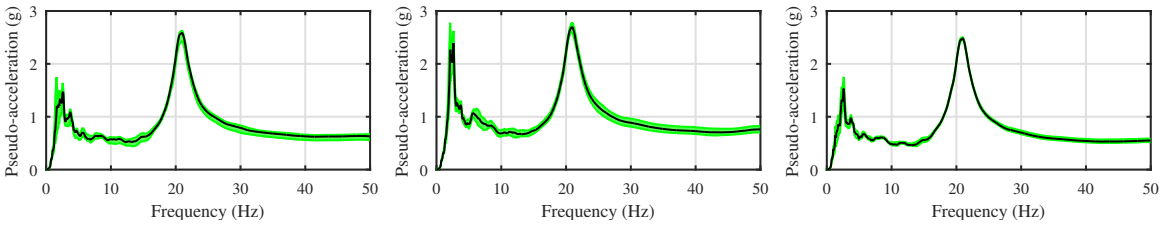

(a) 1D modelling strategy. (b) 2D modelling strategy. (c) 3D modelling strategy.

Figure 14: Time evolution of the ZPA - 90% confidence interval is depicted in green - BANDIT.

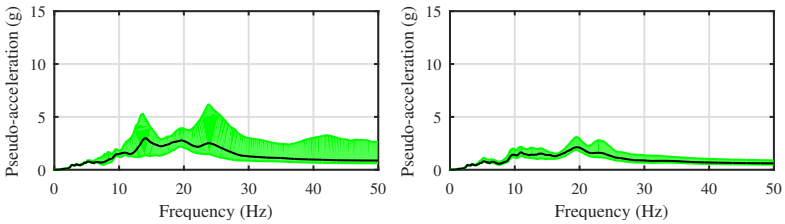

(a) 2D modelling strategy. (b) 3D modelling strategy.

Figure 15: Time evolution of the ZPA - 90% confidence interval is depicted in green - SMART 2013.

(a) BANDIT specimen.

(b) SMART 2013 specimen.

Figure 16: Coefficients of variation associated to each selected EDP.

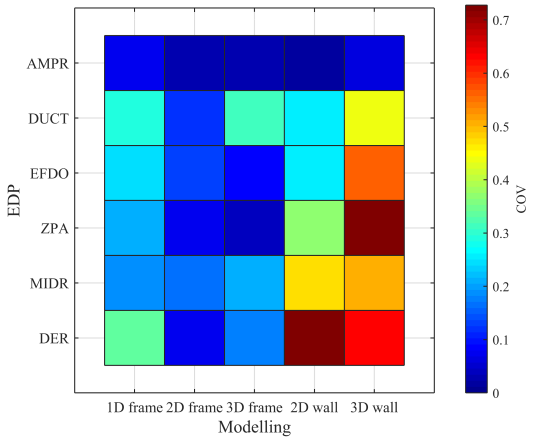

Figure 17: Covariance matrix.

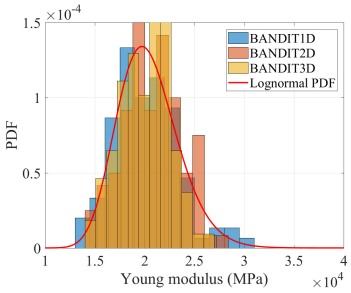

(a) Young modulus.

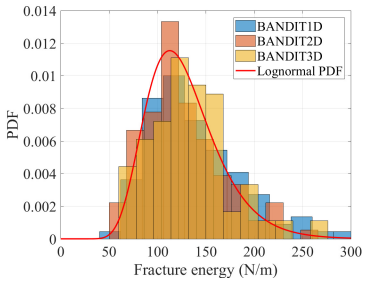

(b) Fracture energy.

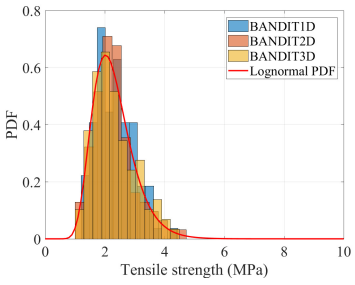

(c) Tensile strength.

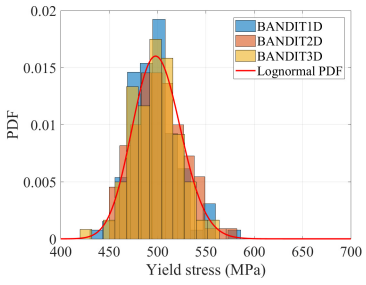

(d) Yield stress.

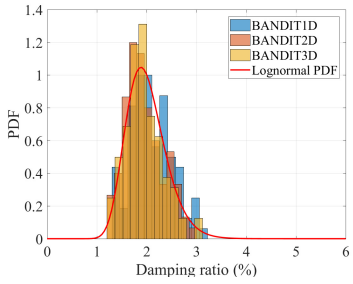

(e) Damping ratio.

Figure 18: Histograms of the realizations of the input parameters - BANDIT case-study.

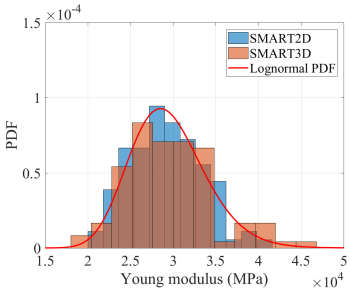

(a) Young modulus.

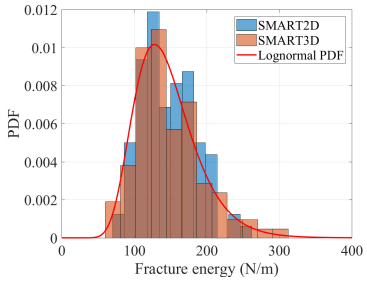

(b) Fracture energy.

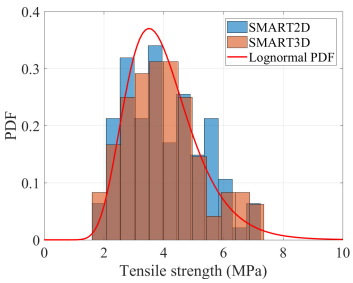

(c) Tensile strength.

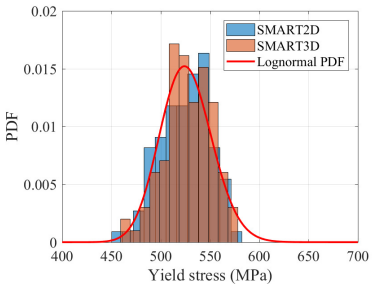

(d) Yield stress.

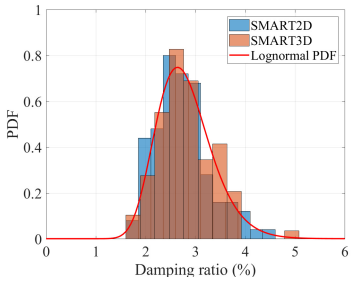

(e) Damping ratio.

Figure 19: Histograms of the realizations of the input parameters - SMART 2013 case-study.

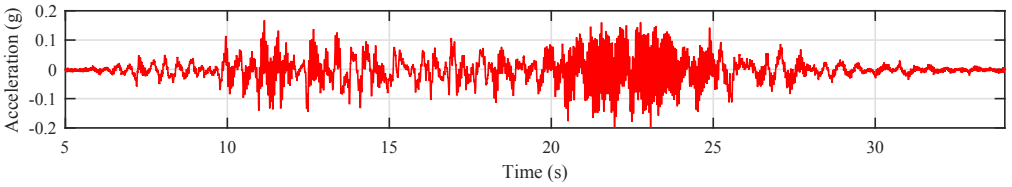

(a) BANDIT - X direction.

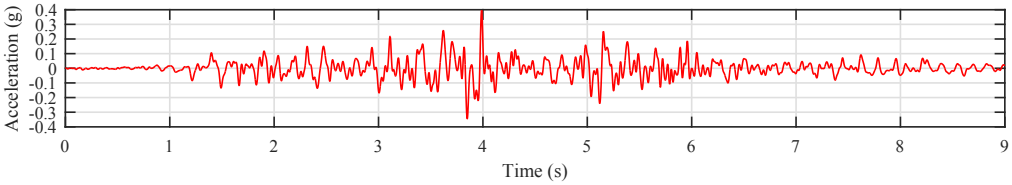

(b) SMART 2013 - X direction.

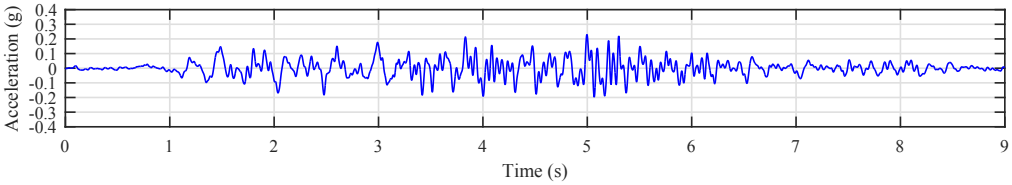

(c) SMART 2013 - Y direction.

Figure 20: Input accelerograms used for BANDIT and SMART 2013.